Materials for Renewable and Sustainable Energy (2022) 11:131–141
https://doi.org/10.1007/s40243-022-00212-5

ORIGINAL PAPER

Valorization of the inedible pistachio shells into nanoscale transition metal and nitrogen codoped carbon-based electrocatalysts for hydrogen evolution reaction and oxygen reduction reaction

Mohsin Muhyuddin[1] · Nicolo' Zocche[1] · Roberto Lorenzi[1] · Chiara Ferrara[1] · Federico Poli[2] · Francesca Soavi[2] · Carlo Santoro[1]

Received: 21 April 2022 / Accepted: 5 July 2022 / Published online: 13 July 2022

Abstract
Making a consistency with the objectives of circular economy, herein, waste pistachios shells were utilized for the development of hydrogen evolution reaction (HER) and oxygen reduction reaction (ORR) electrocatalysts which are the key bottleneck in the technological evolution of electrolyzers and fuel cells, respectively. As an alternative to scarce and expensive platinum-group-metal (PGM) electrocatalysts, metal nitrogen carbons (MNCs) are emerging as a promising candidate for both aforementioned electrocatalysis where iron and nickel are the metal of choice for ORR and HER, respectively. Therefore, FeNCs and NiNCs were fabricated utilizing inedible pistachio shells as a low-cost biosource of carbon. The steps involved in the fabrication of electrocatalyst were correlated with electrochemical performance in alkaline media. Encouraging onset potential of ~ 0.88 V vs RHE with a possibility of a 2 + 2 reaction pathway was observed in pyrolyzed and ball-milled FeNC. However, HF etching for template removal slightly affected the kinetics and eventually resulted in a relatively higher yield of peroxide. In parallel, the pyrolyzed NiNC demonstrated a lower HER overpotential of ~ 0.4 V vs RHE at − 10 mA cm^{-2}. Nevertheless, acid washing adversely affected the HER performance and consequently, very high overpotential was witnessed.

Keywords Waste pistachio · Circular economy · Electrocatalysts · Oxygen reduction reaction · Hydrogen evolution reaction

Introduction

Concerns over foreseeable energy crises and environmental safety launch two major hotspots for researchers of the twenty-first century where finite fossil fuels, climate change and rocketing population growth instigate worldwide geopolitical apprehensions. The energy consumption is expected to reach 27 TW by the year 2050 [1], creating an alarming situation for international stakeholders. In the meantime, large-scale implementation of traditional renewable energy sources seems to be far away from reality owing to their inevitable dependence on specific timeframes and weather conditions [2–4]. Hence, more sustainable, economically viable and eco-friendly alternatives are urgently required to efficaciously address the looming energy crises. At this juncture, hydrogen technologies, (specifically electrolyzers and fuel cells) become more relevant, demonstrating a capacity to overcome energy deficit without contributing to the planetary carbon footprint [4].

Water electrolyzers produce green hydrogen once coupled with renewable energy. Fuel cells utilize hydrogen as a green fuel for the generation of electricity in a reverse electrochemical pathway with zero CO_2 emission [5, 6]. Despite the extraordinary advantages offered by electrolyzers and fuel cells, their commercialization is still unapproachable essentially due to the lethargic kinetics of cathodic reactions involving hydrogen evolution reaction (HER) and oxygen reduction reaction (ORR), respectively [7, 8]. To overcome the kinetic barriers for both aforementioned cathodic reactions, scarce and overpriced platinum-group-metal (PGM) electrocatalysts are employed, constituting

✉ Mohsin Muhyuddin
m.muhyuddin@campus.unimib.it

✉ Carlo Santoro
carlo.santoro@unimib.it

[1] Department of Material Science, University of Milan Bicocca, U5 Via Cozzi 55, 20125 Milan, Italy

[2] Department of Chemistry "G. Ciamician", Alma Mater Studiorum University of Bologna, Via Selmi 2, 40100 Bologna, Italy

the key bottleneck in the given fields [9–11]. Furthermore, PGM electrocatalysts are also notorious for their long-term instability and least tolerance against natural contaminants (mainly anions) [7]. To address these issues, a plethora of scientific endeavors have been invested in the development of robust and efficient PGM-free electrocatalysts for HER and ORR.

In the pursuit of PGMs replacement, atomically dispersed transition metals in nitrogen-doped carbon matrix are capturing scientific attention on the account of their sufficient kinetic activity, stability and aptitude to be operated under less corrosive alkaline conditions [9, 12–14]. Doping of transition metal over a carbonaceous backbone generates electrochemically active sites while the defect-rich carbon framework ensures a conducive platform for catalytic performance [12, 15]. In the past, interesting scientific exertions have been made for metal-carrying carbon electrocatalysts which verify the employment of iron primarily important for ORR electrocatalysis [16–20] while nickel emerges as a suitable option for HER [6, 21–25]. Moreover, in a comparison with other non-PGMs, iron and nickel not only safeguard the cost practicality due to their higher relative abundance, but their utilization in the electrocatalysts is also congruous with the biomimicry of hydrogenases involving iron and/or nickel-based active sites for electrocatalysis [26]. In any case, carbon is an indispensable support material for both PGM and PGM-free electrocatalysts due to its structural flexibility, electronic conductivity, environmental stability and cost-effectiveness [27, 28]. Fabrication of such carbon-based electrocatalysts can be further economized using waste biomasses as readily available and cost-effective carbon sources [28]. Carbon recovery from waste products itself is an important research topic within the core of circular economy where derived carbon-based nanomaterials could find their diverse application in the arena of energy conversion and storage [29–32]. It is an astonishing fact that annually more than 140 billion metric tons of biomass are gathered all over the world in the form of agricultural waste [33]. Therefore, valorization of waste biomass into useful and cost-effective nanomaterials through pyrolysis could be a lucid idea considering the rewards of ecological wellbeing [34]. For that reason, a huge scientific interest in biomass-derived HER and ORR electrocatalysts has been witnessed in the past few years [28, 29, 34–37].

Cultivation of pistachio (*Pistacia vera*) has increased in demand since this nutritious fruit offers multiple health benefits. According to the statistics of the International Nut and Dried Fruit Council (INC), global pistachios (in-shell) production was figured more than 1 million metric tons in the season of 2020/2021 with a 68% upsurge over the harvesting of the former decade [38]. However, a massive amount of leftover shells with no economic value is accumulated after the processing of the crop. The transformation of these waste pistachio shells into carbon-based electrocatalysts can open up a new window into the paradigm of green energy. In recent times, pistachio shells have been utilized as a carbon precursor for electrode applications in the domain of energy storage and a few worth reading examples can be found in the literature [39–44]. Recently, Benítez et al. reported pistachio shells derived activation carbon as an efficient sulfur host for lithium-sulfur batteries owing to its extraordinary textural characteristics befitting for electrochemical reactions [40]. Furthermore, Sciarria et al. attempted to produce metal-free activated biochar using pistachio shells as a feedstock and analyzed the ORR activity in neutral media which is essential for the microbial fuel cell [45]. Additionally, Sumboja and co-workers formulated an interesting study to fabricate FeCo-loaded and nitrogen-functionalized carbon-based electrocatalyst for ORR in aluminum-air batteries that exhibited outstanding onset potential of 0.93 V vs. RHE (reversible hydrogen potential) [39].

Satisfactory characteristics of carbonaceous nanomaterials derived from inedible pistachio shells motivate the commencement of a systematic study for the fabrication of HER and ORR electrocatalysts employing pistachio shells as a key carbon source. Very recently our research group has reported the transformation of waste face surgical masks into nanostructured electrocatalysts for fuel cells and electrolyzers through pyrolysis and subsequent functionalization of char with metal phthalocyanine of choice [46]. However, still, a systematic study is required to closely elucidate the steps involve in the quest of atomically dispersed metal–nitrogen–carbon (MNC) electrocatalysts of two different natures but utilizing the same biosource carbon because metal doping route and followed fabrication steps can directly affect the catalytic performance. Herein, we report the synthesis of HER and ORR electrocatalysts through pyrolysis of waste pistachio shells. For the fabrication of HER electrocatalysts, nickel and nitrogen doping was carried out whereas ORR electrocatalysts were produced after co-doping of iron and nitrogen. Effects of synthesis conditions such as high-temperature pyrolysis, ball milling and acid washing, on the overall electrochemical performance in the alkaline medium, were closely analyzed. Both classes of the developed electrocatalysts exhibited optimistic performance, however, the involved fabrication steps influenced the activities. The study provides a rationale for the prospective research and developments in biomass-derived electrocatalysts within the core of the circular economy.

Materials and methods

Development of electrocatalysts

Pistachios were purchased from a local supermarket and their inedible shells (without nuts) were directly utilized in

the study. To begin with, fully dried pistachio shells were ground into a fine powder using a coffee grinder and subsequently used as a carbon precursor in the pyrolysis treatment. All the chemicals and reagents used in the experimentation were of analytical grade and were used without further processing.

Synthesis of ORR electrocatalysts

In the fabrication of the ORR electrocatalyst, fumed silica (AEROSIL® OX 50) was used as a templating agent to guarantee the formation of micro-mesoporous architecture inside the final electrocatalyst. Well-dispersed micro-mesoporosity is particularly important for ORR electrocatalysis to enhance the number of active sites and ensure the oxygen mass transport to the electroactive moieties which eventually uplift the kinetics of oxygen electro-reduction [7, 47, 48]. Such kind of structure in the final electrocatalyst can be effectively achieved using silica as a sacrificial hard template which can be removed by post-pyrolysis etching treatment [49, 50]. In the first step, all the raw materials were homogeneously mixed using a mortar grinder in a definite weight proportion i.e. 70% powdered pistachio shells, 20% silica, 5% iron nitrate nonahydrate (Alfa Aesar) and 5% nicarbazin (Sigma). Here, iron nitrate nonahydrate and nicarbazin were used as iron and nitrogen source, respectively. The mixture obtained was then transferred into a clean ceramic crucible and was subjected to pyrolysis using a tube furnace (Carbolite). The pyrolysis temperature was maintained at 900 °C for one hour with heating and cooling ramp rates of 300 °C h^{-1} while the whole procedure was carried out under a continuous flow of nitrogen (100 cm^3 min^{-1}). Once the treatment was completed and the room temperature was reached, the black powder was taken out of the furnace and named as FeNC_P. In the next step, the sample was thoroughly homogenized by giving a round of ball milling (E_{MAX}, Retsch Gmbh, Germany) for one hour at 400 rpm to atomically disperse the active moieties. The sample achieved in the second stage was labeled as FeNC_PM. Finally, the obtained fine powder was leached in the in-house prepared 40% solution (20 ml) of hydrofluoric acid (Sigma) for three days at room temperature to remove the silica templating agent and coarser metallic nanoparticles. Upon the completion of the acid leaching step, the electrocatalyst was washed with plentiful Milli-Q water until the neutral pH was achieved and then was fully dried in a vacuum oven. The catalyst obtained at this stage was named FeNC_PME.

Synthesis of HER electrocatalysts

The fabrication procedure adopted for the HER electrocatalysts was similar to that of ORR electrocatalysts except for the involvement of a silica template. Very high microporosity during HER is not desired because it not only leads to the accumulation of gaseous hydrogen which in turn reduces the interface between active moieties and the electrolyte but may also cause the eventual failure of the electrocatalyst. For the synthesis of HER electrocatalyst, the powdered pistachio shells, nickel nitrate hexahydrate (Sigma) and nicarbazin were mixed in a weight proportion of 90%, 5% and 5%, respectively, using a mortar grinder. The mixture was then subjected to pyrolysis with conditions similar to those used for ORR electrocatalysts. After cooling, the pyrolyzed powder was called NiNC_P. Later on, some portion of this sample was ball-milled at 400 rmp for 1 h and named as NiNC_PM. Finally, to leach out the metallic nanoparticles, the electrocatalyst was washed with boiling 0.5 M sulfuric acid for 15 min. After thoroughly washing with an ample quantity of Milli-Q water (until pH 7), the sample was fully dried in a vacuum oven and was labeled as NiNC_PMA. The description of both ORR and HER samples fabricated in the study is summarized in Table 1.

Electrochemical analysis

Ink preparation

The ink was prepared by mixing 4.5 mg of the as-synthesized electrocatalyst with 985 µl isopropanol (Alfa Aesar) followed by the addition of 15 µl of 5.0 wt.% Nafion® D-520 (Alfa Aesar) using a micropipette. Afterwards the suspension was agitated for 10 min using a probe sonicator. Lastly, the vials enclosing inks were further homogenized using ultrasonic bath sonication for half an hour.

ORR evaluation

ORR activity was analyzed through a rotating ring disk electrode (RRDE, Pine WaveVortex) connected with a Pine bipotentiostat. Three-electrodes system was comprising of a working electrode, a counter electrode of platinum wire and a saturated calomel electrode (SCE) as a reference electrode. The working electrode was fabricated by

Table 1 Nomenclature of the electrocatalysts studied and the synthesis steps done

Samples	Pyrolysis	Ball milling	HF etching	Washing with 0.5 M H_2SO_4
FeNC_P	✓			
FeNC_PM	✓	✓		
FeNC_PME	✓	✓	✓	
NiNC_P	✓			
NiNC_PM	✓	✓		
NiNC_PMA	✓	✓		✓

precisely drop-casting the prepared ink on the disk of the RRDE (E6R2 series) having an area of 0.2376 cm^2. The collection efficiency (N) and area of Pt ring (used for the detection of peroxide formed during ORR) were 38% and 0.2356 cm^2, respectively. In this study, two mass loadings of electrocatalysts i.e. 0.2 mg cm^{-2} and 0.6 mg cm^{-2} ware employed for ORR. Linear sweep voltammograms (LSVs) were acquired at the scan rate of 5 mV s^{-1} in the potential window between 0.15 and − 1.05 V vs SCE, while the ring potential was set to be at 0.15 V vs SCE. ORR activity was performed in an oxygen-saturated alkaline medium containing 0.1 M KOH while RRDE was rotating at 1600 rmp. Peroxide formation was estimated using Eq. 1 as follows;

$$\text{Peroxide}(\%) = \frac{200 \times \frac{I_r}{N}}{I_d + \frac{I_r}{N}}, \quad (1)$$

where I_r and I_d are ring current and disk current densities, respectively. Electron transfer number (n) was determined through Eq. 2 as below:

$$n = \frac{4I_d}{I_d + \frac{I_r}{N}}. \quad (2)$$

HER evaluation

Again similar three-electrodes setup was used for the evaluation of HER performance but in nitrogen-saturated 1 M KOH electrolyte solution. This time, the working electrode was prepared by depositing the electrocatalyst ink on the disk of the rotating disk electrode (RDE, E5 series) with a disk area of 0.1963 cm^2, operating at 1600 rpm. Electrocatalyst loading of 0.6 mg cm^{-2} was used to prepare the working electrode. The potential window for acquiring the LSVs (at the scan rate of 5 mV s^{-1}) for HER was maintained between − 1.05 and − 2.05 V vs SCE. During the testing, nitrogen gas was continuously purged in the electrolyte. Eventually, all the potential values were converted into reversible hydrogen potential using the following relationship:

$$E(\text{RHE}) = E(\text{SCE}) + E^0(\text{SCE}) + 0.0591 \times \text{pH}. \quad (3)$$

Characterization tools

Elementar Vario Microcube Device was employed to perform CHNS elemental analysis by keeping the oxidation tube at 850 °C while the combustion tube at 1100 °C. Energy-dispersive X-ray fluorescence (XRF) qualitative analysis was performed using a Bruker Artax 200 spectrometer, equipped with an X-ray tube with Mo anode. X-rays diffraction (XRD, Rigaku Miniflex 600) was employed in the 2θ range of 10°–80° to analyze the crystal structure using the copper source. Carbon structure was studied using LabRam Raman spectroscopy (Jobin Yvon, France) with an excitation wavelength of 632.8 nm (helium–neon laser). The laser was focused on the sample with the help of a microscope (BX40, Olympus, Japan) installed with a 50× Long-Working-Distance objective (0.6 N.A.) while the signals collection was carried out with the help of silicon CCD (Sincerity, Jobin Yvon, France).

Results and discussion

Elemental identification of the developed samples was carried out through XRF and CHNS analysis. From the XRF spectra, shown in Fig. 1, all the samples contain Cl, K and Ca as impurity artifacts that formerly belonged to the original composition of the pistachios shell as unveiled in the XRF spectrum of raw pistachios shells (inset of Fig. 1a). Interestingly, all the ORR and HER electrocatalysts were qualified for the presence of Fe and Ni, respectively, which are metals of interest for the given type of electrocatalysis. The peaks correspond to Si, initially present in the FeNC_P and FeNC_PM, disappeared after the HF etching indicating the successful removal of the templating agent. Since nitrogen is an equally important constituent of the electrocatalysts, its presence was further ensured by performing CHNS analysis and the observation is tabularized in Table 2. CHNS analysis endorses the availability of nitrogen in each functionalized sample.

The XRD analysis evidences the effectiveness of the synthesis of the Fe- and Ni-based electrocatalysts. The evolution of the phase composition following the thermal treatment, milling, and acidic etching is reported in Fig. 2 for both the Fe- and Ni- containing samples. For the FeNC_P sample, it is possible to identify the presence of amorphous components with peaks at ~ 22° and 44°, compatible with the presence of amorphous carbon, as already reported for samples obtained under similar conditions [51] and amorphous silica (see gray pattern in the upper panel as reference). The observed sharp peaks can be associated with the presence of crystalline cristobalite (reference ICSD 98-004-7220) and are compatible also with a small fraction of crystalline iron (ICSD 98-018-5731). The partial crystallization of the amorphous silica can be driven by the presence of other components such as metal impurities and the presence of carbon, as already observed [52, 53]. For the scope of the present study, the partial recrystallization of the silica component is not a problem since silica was employed just as a hard template. The milling of the powders does not affect the phase composition, as evident from the comparison of the patterns of FeNC_P and FeNC_PM. The effectiveness of the HF etching is demonstrated by the pattern obtained for the

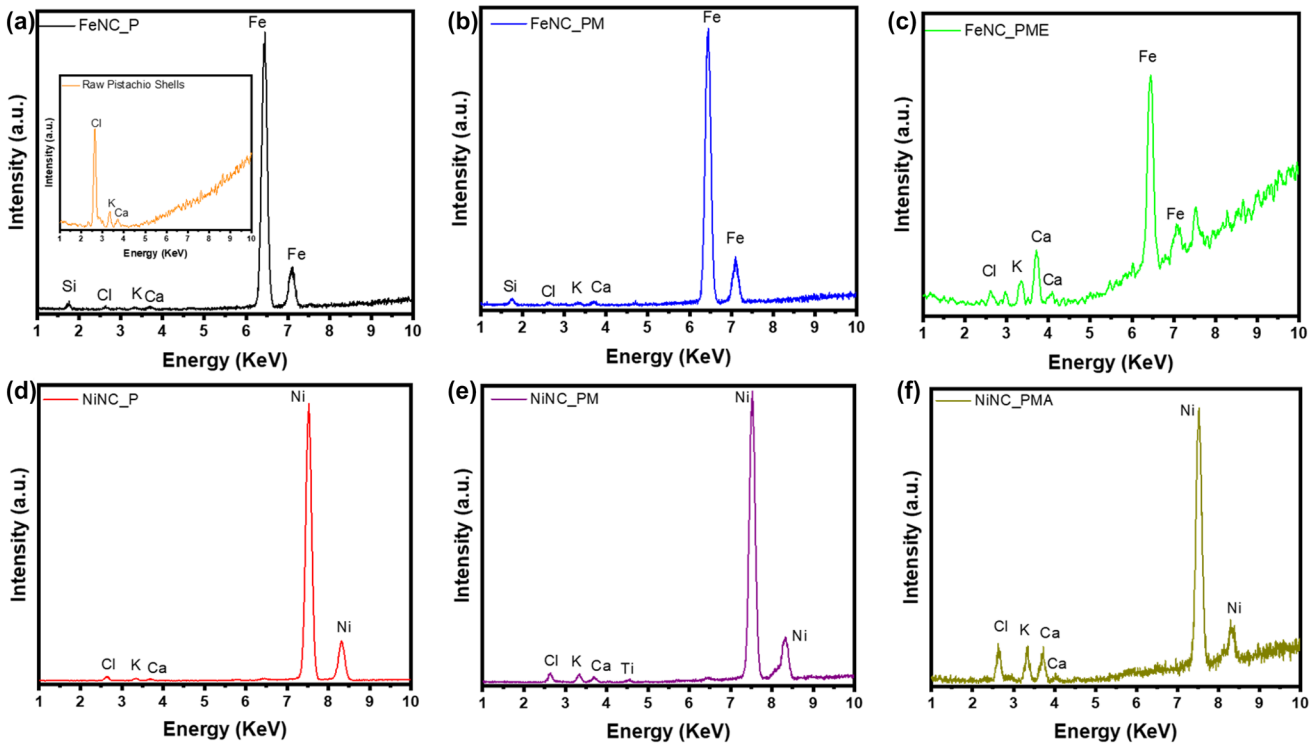

Fig. 1 XRF spectra of **a** FeNC_P, **b** FeNC_PM, **c** FeNC_PME, **d** NiNC_P, **e** NiNC_PM, and **f** NiNC_PMA, whereas XRF spectrum of raw pistachio shells is given in the inset of **a**

Table 2 CHNS analysis of the raw pistachio shells and derived samples

Samples	Carbon (%)	Hydrogen (%)	Nitrogen (%)	Sulfur (%)
Raw pistachio shells	48.66	5.922	1.27	0.065
FeNC_P	12.23	0.088	2.12	0.167
FeNC_PM	59.91	0.802	2.70	0.117
FeNC_PME	87.93	1.563	3.40	0.114
NiNC_P	74.79	1.319	2.15	0.179
NiNC_PM	83.82	1.232	2.41	0.226
NiNC_PMA	86.93	1.350	2.48	0.212

FeNC_PME for which the peaks of cristobalite are no more observed. Also the broad contributions related to amorphous components results shifted, supporting the hypothesis that the amorphous silica has been removed leaving only the amorphous carbon fraction, as demonstrated also by Raman data (see Fig. 3). No peaks associated with crystalline Fe are observed; this result, in combination with data from XRF, supports the hypothesis that the iron is atomically dispersed within the carbon matrix.

Similar results for the final step are obtained also for the Ni-based HER electrocatalysts, nevertheless, the intermediate obtained phases are different. The differences in the phase composition of FeNC_P and NiNC_P samples can be rationalized considering the presence of 20 wt.% of silica templating agent only in the FeNC_P sample and with the different reactivity of Fe and Ni. Indeed, the NiNC_P pattern shows broad reflections associated with amorphous carbon and sharp reflections compatible with the presence of metal Ni (ICSD 98-007-6667). KNiF3 (ICSD 98-005-6098) and a small amount of quartz (ICSD 98-020-0728). The presence of the KNiF3 is compatible with the results obtained from XRF. The milling step, similarly to the case of Fe samples, does not affect the composition as evident from the inspection of NiNC_P and NiNC_PM patterns. The reduction of the intensities of the peaks associated with Ni can be explained by a size reduction of the particles; indeed, a broadening can be observed. Finally, the acidic etching promotes the removal of coarse metal particles as peaks of metal Ni is not detected. The peaks associated with $KNiF_3$

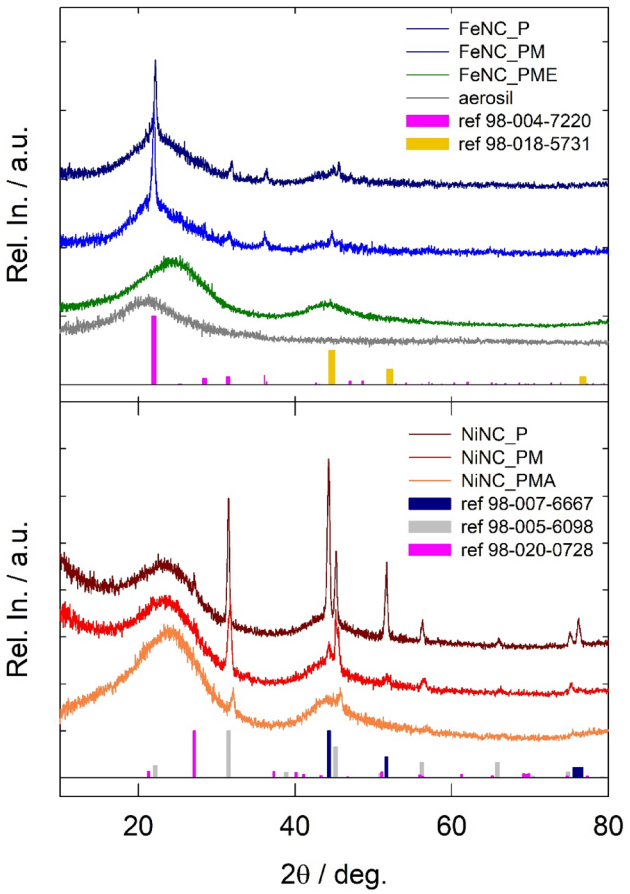

Fig. 2 Powder X-rays diffraction data for the Fe- and Ni-based series of samples; reference patterns as vertical bars for data from database and gray pattern obtained for the pristine fumed silica (templating agent) used in the preparation of Fe-based compositions

are strongly reduced suggesting that also this component has been partially removed.

Carbon structures of the derived electrocatalysts were studied through Raman spectroscopy and the acquired spectra are reported in Fig. 3. All the Raman spectra primarily exhibited the two typical peaks of D-band and G-band approximately centered at 1330 cm^{-1} and 1590 cm^{-1}, respectively. G-band is a characteristic feature of the sp^2 graphitic domains with the in-plane motion of carbon atoms with E_{2g} symmetry while breathing modes with A_{1g} symmetry give rise to D-band [54]. Defect-induced D-band is often missing in the case of ideal graphite and emerges mainly due to the presence of graphitic disorders and structural discontinuities. Hence, defects located in the carbon structure can be monitored by evaluating the D-band. All the ORR and HER electrocatalysts had decidedly dominant D peaks, emphasizing the existence of defect-rich structure. It is important to mention that inherent or induced carbon defects provide strong electrocatalytic actives sites for ORR activity [15, 55, 56], moreover such defects also show a positive contribution toward HER [57]. ID/IG ratio is a conventional descriptor to quantify the defect density. Interesting ID/IG remained nearly the same for all the three ORR electrocatalysts and its value was slightly higher than 1, confirming the numerousness of graphitic defects. On the other hand, NiNC_P and NiNC_PMA showed the highest ID/IG ratio nearly equal to 1.2 which was marginally reduced during the ball milling, specifying a minor upsurge in the graphitization degree.

ORR activity

Finally, the ORR activities of prepared FeNCs were investigated by performing RRDE measurements in oxygen-rich 0.1 M KOH at 1600 rpm and the achieved trends are displayed in Fig. 4. To further analyze the effect of electrocatalyst loading, RRDE based working electrode was configured with a deposition of 0.2 mg cm^{-2} and 0.6 mg cm^{-2} of electrocatalyst on the disk. From the LSVs, FeNC_PM exhibited maximum onset potential (E_{onset}) at the current density of -0.1 mA cm^{-2} which is a benchmark value utilized for identifying the overpotentials towards ORR. The onset potential of FeNC_PM with 0.6 mg cm^{-2} loading was found to be at ~ 0.88 V vs RHE. The electrocatalysts loading on RRDE displayed an obvious effect on the reaction kinetics where the $E_{1/2}$, in any case, shifted positively as the electrocatalysts loading was threefold increased. However, the acid etching showed contrary effects on the overall activity where the onset potential was slightly delayed (0.83 V vs RHE) with a certain drop in current density. The half-wave potential ($E_{1/2}$) estimated using the first differential method came out to be approximately at 0.63 V, 0.7 V and 0.7 V for FeNC_P, FeNC_PM and FeNC_PME respectively, with electrocatalyst loading of 0.2 mg cm^{-2}, however, the corresponding $E_{1/2}$ values eventually increased to 0.7 V, 0.75 V and 0.74 V when loading of 0.6 mg cm^{-2} was employed.

All the FeNC samples initially showed a rising trend in the corresponding ring current densities however, after 0.6 V vs RHE the ring current densities of FeNC_P and FeNC_PM started declining as the overpotential increased and a more pronounced effect was observed for the higher loading. An obvious upshot of this phenomenon was reflected in the peroxide yield which was significantly reduced as the overpotential increased. Based upon this observation, it can be speculated that FeNC_P and FeNC_PM possess peroxide self-scavenging active sites. This means that the peroxide produced at lower overpotential is subsequently reduced at higher overpotential on the secondary active sites, confirming the possibility of a 2 + 2 reduction pathway. Generally, higher loading depresses the peroxide yield [58] probably due to the reduction occurring within the thicker electrocatalysts layer [59, 60]. The electron transfer number estimated for FeNC_P and FeNC_PM were more or less similar and resulted to be their maximum with a loading of 0.6 mg cm^{-2}

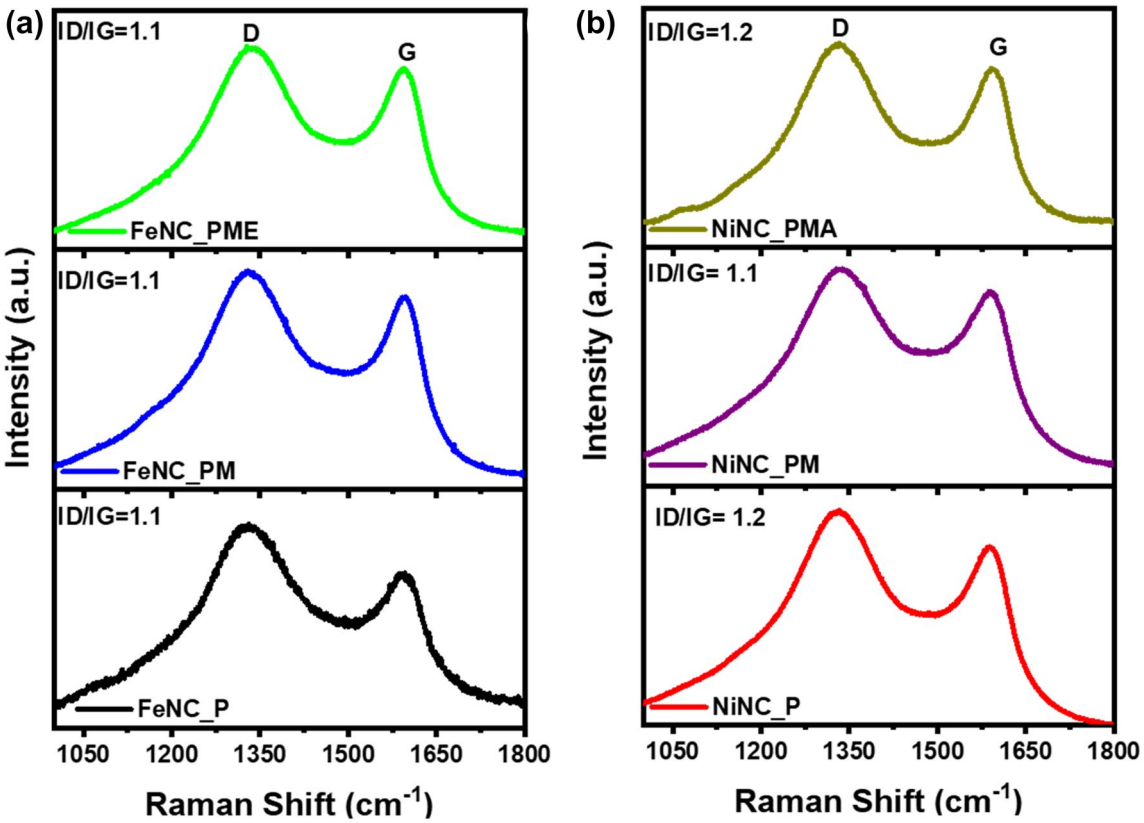

Fig. 3 Illustrating the Raman spectra of **a** FeNCs for ORR and **b** NiNCs for HER electrocatalysis

(Fig. 4d). Both electrocatalysts exhibited the number of electron transfer close to ~ 3.5 at higher overpotentials. On the other side, the acid-etched sample (FeNC_PME) yielded a relatively lower percentage of peroxide in the beginning but after ~ 0.45 V vs RHE peroxide production increases together with a slight decrement in the electron transference compared to the other samples. A possible reason for the diminishing of ORR activity in the case of FeNC_PME could be the acid treatment that undesirably removed some of the active iron species, leaving the less active electrocatalyst behind. Previously, a marked decrease in the ORR performance of FeNCs due to acid treatment has been witnessed which turned out in a loss of iron-carrying active sites [61], however, the effect of acid treatment on the ORR performance is more related to the nature of electrocatalyst developed [61, 62]. In our case, acid etching did not disturb the kinetics of ORR but altered the reaction pathway, particularly by producing more peroxide at higher potentials.

HER activity

To evaluate the HER performance of the developed NiNC electrocatalysts in alkaline media (N_2 purged 1 M KOH), HER measurements were obtained using a typical three-electrode system where the working electrode was configured by drop-casting 0.6 mg cm^{-2} on the glassy carbon disk of RDE. Polarization curves obtained at the scan rate of 5 mV s^{-1} together with their corresponding Tafel plots are presented in Fig. 5. Among all the three fabricated electrocatalysts, NiNC_P demonstrated the best HER performance. In terms of E_{onset}, the results showed the following order of NiNC_P > NiNC_PM > > NiNC_PMA. As compared to NiNC_P the HER performance seems to be nearly twofold reduced after acid washing, which could be linked with the removal of nickel content. The overpotential estimated at the current density of − 10 mA cm^{-2} was lowest for NiNC_P with a value of 403 mV (RHE) and slightly increased by 5 mV in the case of NiNC_PM. However, the overpotential estimated for NiNC_PMA was significantly raised to 693 mV (RHE). The Tafel plots provide complementary insights into the HER kinetics. The lowest Tefal slope of sample NiNC_P (146 mV/dec) highlights its fast kinetics compared to other counterparts. Conversely, the highest Tafel slope was estimated for NiNC_PMA (~ 247 mV/dec) endorses the ineffectiveness of the acid washing towards HER performance. This conjecture is consistent with the sequel of XRD analysis which categorically indicated the removal of nickel-based active moieties.

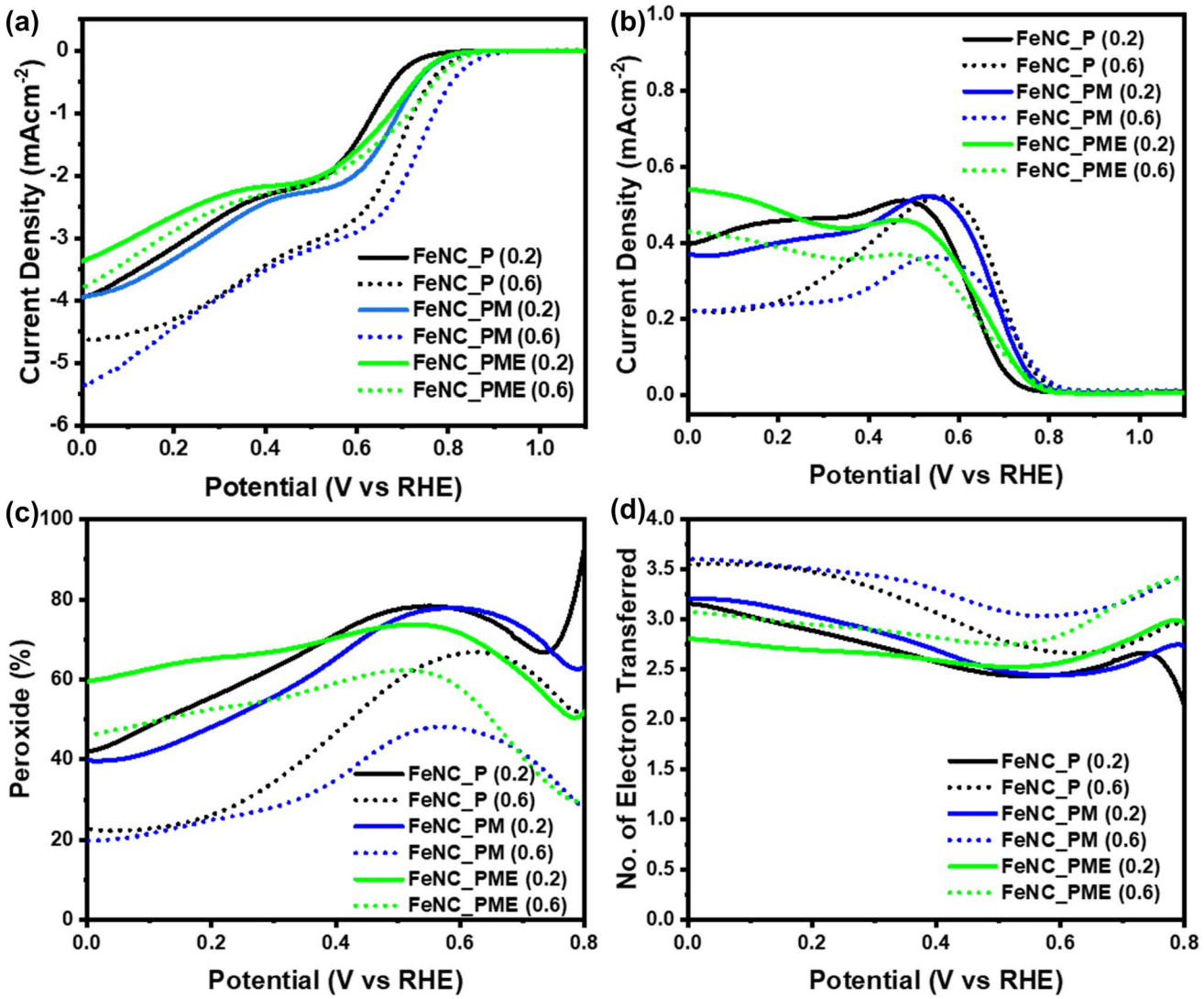

Fig. 4 RRDE analysis of pistachio shells derived FeNCs for ORR in O_2-saturated 0.1 M KOH with 1600 rpm with electrocatalysts loadings of 0.2 and 0.6 mg cm^{-2}; **a** Linear sweep voltammograms (LSVs) at 5 mV s^{-1}, **b** ring current density, **c** peroxide yield and **d** number of electron transfer

Conclusion

In the present study, inedible pistachio shells carrying almost no economic worth were utilized to fabricate MNCs electrocatalysts after functionalizing with iron and nickel for ORR and HER electrocatalysis, respectively, in alkaline media. The typical fabrication steps, particularly pyrolysis, ball milling and acid treatment differently affected the observed activities. The highest ORR E_{onset} and $E_{1/2}$ of 0.88 V and 0.75 V, respectively, were encountered for FeNC_PM and the corresponding values marginally reduced to 0.83 V and 0.74 V in the case of FeNC_PME with electrocatalyst loading of 0.6 mg cm^{-2}. FeNC_P and FeNC_PM emerged as peroxide self-consuming electrocatalysts underlying the possibility of a 2 + 2 reduction pathway while the peroxide production at higher potential got increased with FeNC_PME. A similar trend was observed for HER electrocatalysis, where NiNC_P outperformed the other counterparts with a relatively lower overpotential of 403 mV. The outcomes justify the utilization of inedible waste products like pistachio shells for the economic fabrication of PGM-free electrocatalysts considering them cheaper carbon sources. Nevertheless, further optimization and improvements within the domain of circular economy are obviously necessary to uplift the performance comparable to the state-of-the-art electrocatalysts.

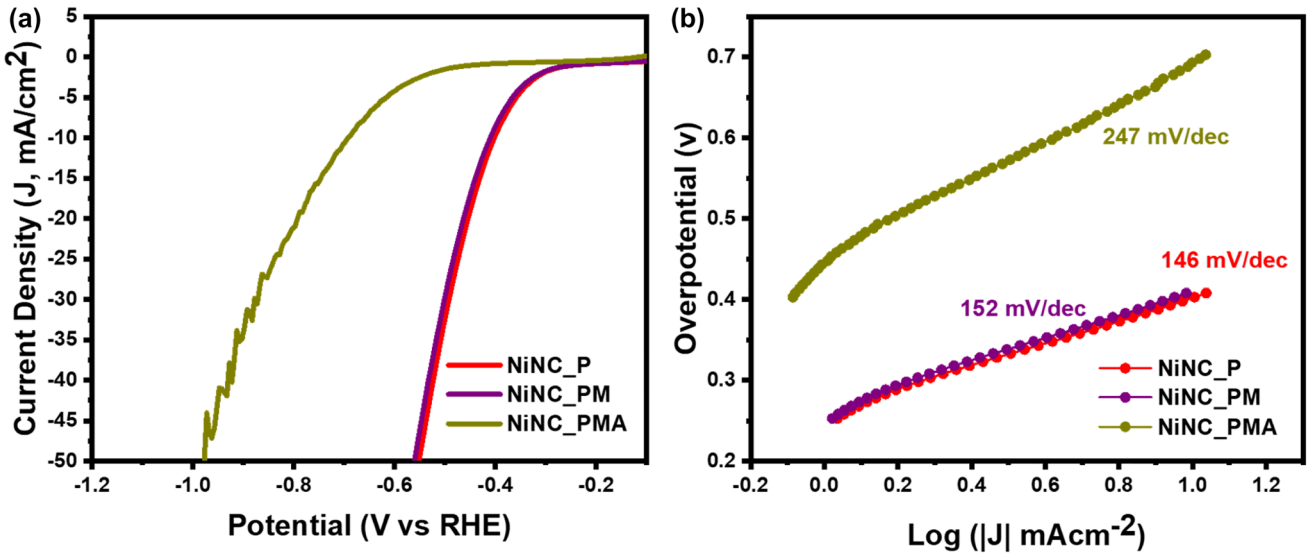

Fig. 5 HER measurements using RDE at 1600 rpm in nitrogen-saturated 1 M KOH **a** LSVs at 5 mV s^{-1} and **b** corresponding Tafel plots

Acknowledgements CS would like to thank the support from the Italian Ministry of Education, Universities and Research (Ministero dell'Istruzione, dell'Università e della Ricerca – MIUR) through the "Rita Levi Montalcini 2018" fellowship (Grant number PGR18MA-ZLI). RL would like to thank the support from University of Milano-Bicocca through grant "Bando Infrastrutture di Ricerca – Edizione 2021".

Declarations

Conflict of interest Authors have no conflict of interest to declare.

References

1. Lewis, N.S., Nocera, D.G.: Powering the planet: chemical challenges in solar energy utilization. PNAS **103**, 15729–15735 (2006). https://doi.org/10.1073/pnas.0603395103
2. Woyte, A., Van Thong, V., Belmans, R., Nijs, J.: Voltage fluctuations on distribution level introduced by photovoltaic systems. IEEE Trans. Energy Convers. **21**, 202–209 (2006). https://doi.org/10.1109/TEC.2005.845454
3. Sherif, S.A., Barbir, F., Veziroglu, T.N.: Wind energy and the hydrogen economy—review of the technology. Sol. Energy **78**, 647–660 (2005). https://doi.org/10.1016/j.solener.2005.01.002
4. Ďurovič, M., Hnát, J., Bouzek, K.: Electrocatalysts for the hydrogen evolution reaction in alkaline and neutral media. A comparative review. J. Power Sources **493**, 229708 (2021). https://doi.org/10.1016/j.jpowsour.2021.229708
5. Sultan, S., Tiwari, J.N., Singh, A.N., Zhumagali, S., Ha, M., Myung, C.W., Thangavel, P., Kim, K.S.: Single atoms and clusters based nanomaterials for hydrogen evolution, oxygen evolution reactions, and full water splitting. Adv. Energy Mater. **9**, 1900624 (2019). https://doi.org/10.1002/aenm.201900624
6. Vij, V., Sultan, S., Harzandi, A.M., Meena, A., Tiwari, J.N., Lee, W.-G., Yoon, T., Kim, K.S.: Nickel-based electrocatalysts for energy-related applications: oxygen reduction, oxygen evolution, and hydrogen evolution reactions. ACS Catal. **7**, 7196–7225 (2017). https://doi.org/10.1021/acscatal.7b01800
7. Ouyang, C., Wang, X.: Recent progress in pyrolyzed carbon materials as electrocatalysts for the oxygen reduction reaction. Inorg. Chem. Front. **7**, 28–36 (2019). https://doi.org/10.1039/C9QI00962K
8. Wang, J., Xu, F., Jin, H., Chen, Y., Wang, Y.: Non-noble metal-based carbon composites in hydrogen evolution reaction: fundamentals to applications. Adv. Mater. **29**, 1605838 (2017). https://doi.org/10.1002/adma.201605838
9. Meng, Y., Huang, X., Lin, H., Zhang, P., Gao, Q., Li, W.: Carbon-based nanomaterials as sustainable noble-metal-free electrocatalysts. Front. Chem. (2019). https://doi.org/10.3389/fchem.2019.00759
10. Wang, T., Xie, H., Chen, M., D'Aloia, A., Cho, J., Wu, G., Li, Q.: Precious metal-free approach to hydrogen electrocatalysis for energy conversion: from mechanism understanding to catalyst design. Nano Energy **42**, 69–89 (2017). https://doi.org/10.1016/j.nanoen.2017.10.045
11. Pan, J., Yu, S., Jing, Z., Zhou, Q., Dong, Y., Lou, X., Xia, F.: Electrocatalytic hydrogen evolution reaction related to nanochannel materials. Small Struct. **2**, 2100076 (2021). https://doi.org/10.1002/sstr.202100076
12. Chen, M.-X., Tong, L., Liang, H.-W.: Understanding the catalytic sites of metal-nitrogen-carbon oxygen reduction

electrocatalysts. Chem. Eur. J. **27**, 145–157 (2021). https://doi.org/10.1002/chem.202002427
13. Baghban, A., Habibzadeh, S., Zokaee Ashtiani, F.: On the evaluation of hydrogen evolution reaction performance of metal-nitrogen-doped carbon electrocatalysts using machine learning technique. Sci. Rep. **11**, 21911 (2021). https://doi.org/10.1038/s41598-021-00031-0
14. Sgarbi, R., Kumar, K., Jaouen, F., Zitolo, A., Ticianelli, E.A., Maillard, F.: Oxygen reduction reaction mechanism and kinetics on M-NxCy and M@N-C active sites present in model M-N-C catalysts under alkaline and acidic conditions. J Solid State Electrochem. **25**, 45–56 (2021). https://doi.org/10.1007/s10008-019-04436-w
15. Yan, D., Li, Y., Huo, J., Chen, R., Dai, L., Wang, S.: Defect chemistry of nonprecious-metal electrocatalysts for oxygen reactions. Adv. Mater. **29**, 1606459 (2017). https://doi.org/10.1002/adma.201606459
16. Wang, W., Jia, Q., Mukerjee, S., Chen, S.: Recent insights into the oxygen-reduction electrocatalysis of Fe/N/C materials. ACS Catal. **9**, 10126–10141 (2019). https://doi.org/10.1021/acscatal.9b02583
17. Liu, Q., Wang, Y., Hu, Z., Zhang, Z.: Iron-based single-atom electrocatalysts: synthetic strategies and applications. RSC Adv. **11**, 3079–3095 (2021). https://doi.org/10.1039/D0RA08223F
18. Asset, T., Atanassov, P.: Iron-nitrogen-carbon catalysts for proton exchange membrane fuel cells. Joule **4**, 33–44 (2020). https://doi.org/10.1016/j.joule.2019.12.002
19. Kramm, U.I., Lefèvre, M., Larouche, N., Schmeisser, D., Dodelet, J.-P.: Correlations between mass activity and physicochemical properties of Fe/N/C catalysts for the ORR in PEM fuel cell via 57Fe Mössbauer spectroscopy and other techniques. J. Am. Chem. Soc. **136**, 978–985 (2014). https://doi.org/10.1021/ja410076f
20. Santoro, C., Bollella, P., Erable, B., Atanassov, P., Pant, D.: Oxygen reduction reaction electrocatalysis in neutral media for bioelectrochemical systems. Nat Catal. **5**, 473–484 (2022). https://doi.org/10.1038/s41929-022-00787-2
21. Wang, Q., Sun, T., Xue, B.: Nickel nanoparticles encapsulated by nitrogen-doped bamboo-shaped carbon nanotubes with a high-level doping: a boosting electrocatalyst for alkaline hydrogen evolution. Appl. Surf. Sci. **564**, 150439 (2021). https://doi.org/10.1016/j.apsusc.2021.150439
22. Lei, C., Wang, Y., Hou, Y., Liu, P., Yang, J., Zhang, T., Zhuang, X., Chen, M., Yang, B., Lei, L., Yuan, C., Qiu, M., Feng, X.: Efficient alkaline hydrogen evolution on atomically dispersed Ni–Nx Species anchored porous carbon with embedded Ni nanoparticles by accelerating water dissociation kinetics. Energy Environ. Sci. **12**, 149–156 (2019). https://doi.org/10.1039/C8EE01841C
23. Oluigbo, C.J., Xu, Y., Louis, H., Yusuf, A.B., Yaseen, W., Ullah, N., Alagarasan, K.J., Xie, M., Ekpenyong, E.E., Xie, J.: Controllable fabrication of abundant nickel-nitrogen doped CNT electrocatalyst for robust hydrogen evolution reaction. Appl. Surf. Sci. **562**, 150161 (2021). https://doi.org/10.1016/j.apsusc.2021.150161
24. Lu, X., Tan, X., Wang, D.-W., Ng, Y.H., Tahini, H.A., Tan, H., Yan, W., Smith, S.C., Amal, R.: Nitrogen doped carbon nanosheets coupled nickel-carbon pyramid arrays toward efficient evolution of hydrogen. Adv. Sustain. Syst. **1**, 1700032 (2017). https://doi.org/10.1002/adsu.201700032
25. Santoro, C., Lavacchi, A., Mustarelli, P., Di Noto, V., Elbaz, L., Dekel, D.R., Jaouen, F.: What is next in anion-exchange membrane water electrolyzers? Bottlenecks, benefits, and future. Chemsuschem **15**, e202200027 (2022). https://doi.org/10.1002/cssc.202200027
26. Zou, X., Zhang, Y.: Noble metal-free hydrogen evolution catalysts for water splitting. Chem. Soc. Rev. **44**, 5148–5180 (2015). https://doi.org/10.1039/C4CS00448E
27. Du, L., Shao, Y., Sun, J., Yin, G., Liu, J., Wang, Y.: Advanced catalyst supports for PEM fuel cell cathodes. Nano Energy **29**, 314–322 (2016). https://doi.org/10.1016/j.nanoen.2016.03.016
28. Du, L., Zhang, G., Liu, X., Hassanpour, A., Dubois, M., Tavares, A.C., Sun, S.: Biomass-derived nonprecious metal catalysts for oxygen reduction reaction: the demand-oriented engineering of active sites and structures. Carbon Energy. **2**, 561–581 (2020). https://doi.org/10.1002/cey2.73
29. Deng, J., Li, M., Wang, Y.: Biomass-derived carbon: synthesis and applications in energy storage and conversion. Green Chem. **18**, 4824–4854 (2016). https://doi.org/10.1039/C6GC01172A
30. Muhyuddin, M., Mustarelli, P., Santoro, C.: Recent advances in waste plastic transformation into valuable platinum-group metal-free electrocatalysts for oxygen reduction reaction. Chemsuschem **14**, 3785–3800 (2021). https://doi.org/10.1002/cssc.202101252
31. Karakoti, M., Pandey, S., Tatrari, G., Sati, S.C., Sahoo, N.G.: Recycling of plastics into advance carbon nanomaterials and their application in energy storage system. In: Parameswaranpillai, J., Mavinkere Rangappa, S., Gulihonnehalli Rajkumar, A., Siengchin, S. (eds.) Recent Developments in Plastic Recycling, pp. 259–281. Springer, Singapore (2021)
32. Munuera, J., Britnell, L., Santoro, C., Cuéllar-Franca, R., Casiraghi, C.: A review on sustainable production of graphene and related life cycle assessment. 2D Mater. **9**, 012002 (2021). https://doi.org/10.1088/2053-1583/ac3f23
33. Converting Waste Agricultural Biomass into a Resource. UNEP, Japan (2009)
34. Borghei, M., Lehtonen, J., Liu, L., Rojas, O.J.: Advanced biomass-derived electrocatalysts for the oxygen reduction reaction. Adv. Mater. **30**, 1703691 (2018). https://doi.org/10.1002/adma.201703691
35. Li, S., Ho, S.-H., Hua, T., Zhou, Q., Li, F., Tang, J.: Sustainable biochar as an electrocatalysts for the oxygen reduction reaction in microbial fuel cells. Green Energy Environ. **6**, 644–659 (2021). https://doi.org/10.1016/j.gee.2020.11.010
36. Wang, Q., Guo, R., Wang, Z., Shen, D., Yu, R., Luo, K., Wu, C., Gu, S.: Progress in carbon-based electrocatalyst derived from biomass for the hydrogen evolution reaction. Fuel **293**, 120440 (2021). https://doi.org/10.1016/j.fuel.2021.120440
37. Zago, S., Bartoli, M., Muhyuddin, M., Vanacore, G.M., Jagdale, P., Tagliaferro, A., Santoro, C., Specchia, S.: Engineered biochar derived from pyrolyzed waste tea as a carbon support for Fe-N-C electrocatalysts for the oxygen reduction reaction. Electrochim. Acta **412**, 140128 (2022). https://doi.org/10.1016/j.electacta.2022.140128
38. Nuts & Dried fruits Statistical YEARBOOK 2020/2021. The International Nut and Dried Fruit Council Foundation (INC) (2021)
39. Sumboja, A., Prakoso, B., Ma, Y., Irwan, F.R., Hutani, J.J., Mulyadewi, A., Mahbub, M.A.A., Zong, Y., Liu, Z.: FeCo nanoparticle-loaded nutshell-derived porous carbon as sustainable catalyst in Al-air batteries. Energy Mater. Adv. (2021). https://doi.org/10.34133/2021/7386210
40. Benítez, A., Morales, J., Caballero, Á.: Pistachio shell-derived carbon activated with phosphoric acid: a more efficient procedure to improve the performance of Li-S batteries. Nanomaterials (Basel). **10**, E840 (2020). https://doi.org/10.3390/nano10050840
41. Xu, S.-D., Zhao, Y., Liu, S., Ren, X., Chen, L., Shi, W., Wang, X., Zhang, D.: Curly hard carbon derived from pistachio shells as high-performance anode materials for sodium-ion batteries. J. Mater. Sci. (2018). https://doi.org/10.1007/s10853-018-2472-4
42. Elanthamilan, E., Rajkumar, S., Merlin, J.P., Jona, D.S., Monisha, K., Meena, B.C.: Effect of decorating cobalt ferrite spinel structures on pistachio vera shell-derived activated carbon on energy storage applications. Electrochim. Acta **359**, 136953 (2020). https://doi.org/10.1016/j.electacta.2020.136953

43. Ou, J., Wang, H., Wang, J., Wu, S.: Porous carbon/Se composite derived from pistachio shell as high-performance Li-Se battery cathode. Chem. Lett. **50**, 1797–1800 (2021). https://doi.org/10.1246/cl.210314
44. Kim, K., Lim, D.G., Han, C.W., Osswald, S., Ortalan, V., Youngblood, J.P., Pol, V.G.: Tailored carbon anodes derived from biomass for sodium-ion storage. ACS Sustain. Chem. Eng. **5**, 8720–8728 (2017). https://doi.org/10.1021/acssuschemeng.7b01497
45. Pepè Sciarria, T., de Oliveira, M.A.C., Mecheri, B., D'Epifanio, A., Goldfarb, J.L., Adani, F.: Metal-free activated biochar as an oxygen reduction reaction catalyst in single chamber microbial fuel cells. J. Power Sources **462**, 228183 (2020). https://doi.org/10.1016/j.jpowsour.2020.228183
46. Muhyuddin, M., Filippi, J., Zoia, L., Bonizzoni, S., Lorenzi, R., Berretti, E., Capozzoli, L., Bellini, M., Ferrara, C., Lavacchi, A., Santoro, C.: Waste face surgical mask transformation into crude oil and nanostructured electrocatalysts for fuel cells and electrolyzers. Chemsuschem (2021). https://doi.org/10.1002/cssc.202102351
47. Bandosz, T.J.: Revealing the impact of small pores on oxygen reduction on carbon electrocatalysts: a journey through recent findings. Carbon **188**, 289–304 (2022). https://doi.org/10.1016/j.carbon.2021.11.071
48. Ferrero, G.A., Preuss, K., Fuertes, A.B., Sevilla, M., Titirici, M.-M.: The influence of pore size distribution on the oxygen reduction reaction performance in nitrogen doped carbon microspheres. J. Mater. Chem. A. **4**, 2581–2589 (2016). https://doi.org/10.1039/C5TA10063A
49. Serov, A., Artyushkova, K., Atanassov, P.: Fe-N-C oxygen reduction fuel cell catalyst derived from carbendazim: synthesis, structure, and reactivity. Adv. Energy Mater. **4**, 1301735 (2014). https://doi.org/10.1002/aenm.201301735
50. Rojas-Carbonell, S., Artyushkova, K., Serov, A., Santoro, C., Matanovic, I., Atanassov, P.: Effect of pH on the activity of platinum group metal-free catalysts in oxygen reduction reaction. ACS Catal. **8**, 3041–3053 (2018). https://doi.org/10.1021/acscatal.7b03991
51. Rajan, A.S., Sampath, S., Shukla, A.K.: An in situ carbon-grafted alkaline iron electrode for iron-based accumulators. Energy Environ. Sci. **7**, 1110–1116 (2014). https://doi.org/10.1039/C3EE42783H
52. Jiang, X., Bao, L., Cheng, Y.-S., Dunphy, D.R., Li, X., Brinker, C.J.: Aerosol-assisted synthesis of monodisperse single-crystalline α-cristobalite nanospheres. Chem. Commun. **48**, 1293–1295 (2012). https://doi.org/10.1039/C1CC15713B
53. Majling, J., Znasik, P., Agrawal, D., Cheng, J., Roy, R.: Conventional and microwave sintering of condensed silica fume. J. Mater. Res. **10**, 2411–2414 (1995). https://doi.org/10.1557/JMR.1995.2411
54. Ferrari, A.C., Robertson, J.: Interpretation of Raman spectra of disordered and amorphous carbon. Phys. Rev. B. **61**, 14095–14107 (2000). https://doi.org/10.1103/PhysRevB.61.14095
55. Yan, X., Jia, Y., Yao, X.: Defects on carbons for electrocatalytic oxygen reduction. Chem. Soc. Rev. **47**, 7628–7658 (2018). https://doi.org/10.1039/C7CS00690J
56. Yang, L., Shui, J., Du, L., Shao, Y., Liu, J., Dai, L., Hu, Z.: carbon-based metal-free ORR electrocatalysts for fuel cells: past, present, and future. Adv. Mater. **31**, 1804799 (2019). https://doi.org/10.1002/adma.201804799
57. Zhang, L., Jia, Y., Yan, X., Yao, X.: Activity origins in nanocarbons for the electrocatalytic hydrogen evolution reaction. Small **14**, 1800235 (2018). https://doi.org/10.1002/smll.201800235
58. Bonakdarpour, A., Lefevre, M., Yang, R., Jaouen, F., Dahn, T., Dodelet, J.-P., Dahn, J.R.: Impact of loading in RRDE experiments on Fe–N–C catalysts: two- or four-electron oxygen reduction? Electrochem. Solid State Lett. **11**, B105 (2008). https://doi.org/10.1149/1.2904768
59. Santoro, C., Kodali, M., Herrera, S., Serov, A., Ieropoulos, I., Atanassov, P.: Power generation in microbial fuel cells using platinum group metal-free cathode catalyst: effect of the catalyst loading on performance and costs. J. Power Sources **378**, 169–175 (2018). https://doi.org/10.1016/j.jpowsour.2017.12.017
60. Rojas-Carbonell, S., Santoro, C., Serov, A., Atanassov, P.: Transition metal-nitrogen-carbon catalysts for oxygen reduction reaction in neutral electrolyte. Electrochem. Commun. **75**, 38–42 (2017). https://doi.org/10.1016/j.elecom.2016.12.011
61. Singh, D., Tian, J., Mamtani, K., King, J., Miller, J.T., Ozkan, U.S.: A comparison of N-containing carbon nanostructures (CNx) and N-coordinated iron–carbon catalysts (FeNC) for the oxygen reduction reaction in acidic media. J. Catal. **317**, 30–43 (2014). https://doi.org/10.1016/j.jcat.2014.05.025
62. Mamtani, K., Singh, D., Dogu, D., Jain, D., Millet, J.-M.M., Ozkan, U.S.: Effect of acid-washing on the nature of bulk characteristics of nitrogen-doped carbon nanostructures as oxygen reduction reaction electrocatalysts in acidic media. Energy Fuels. **32**, 11038–11045 (2018). https://doi.org/10.1021/acs.energyfuels.8b01510